ELSEVIER

Journal of Molecular Catalysis A: Chemical 149 (1999) 169–178

JOURNAL OF MOLECULAR CATALYSIS A: CHEMICAL

www.elsevier.com/locate/molcata

Preparation of $Ni/ZrO_2–SO_4^{2-}$ catalysts by incipient wetness method: effect of nickel on the isomerization of *n*-butane

M. Pérez [a,b], H. Armendáriz [a,*], J.A. Toledo [a], A. Vázquez [a], J. Navarrete [a], A. Montoya [a], Arturo Gárcia [b]

[a] *Instituto Mexicano del Petróleo, STI, Gerencia de Catalizadores, Eje Central Lázaro Cardenas No. 152, 07730 Mexico D.F., Mexico*
[b] *Instituto Politécnico Nacional, ESFM, Edif. 9, UP Adolfo Lopez M., 07730 Mexico D.F., Mexico*

Received 26 June 1998; received in revised form 16 November 1998; accepted 23 February 1999

Abstract

A series of Ni-promoted sulfated zirconia catalysts with different nickel concentration (from 1 to 9.6 wt.%) were prepared by incipient wetness method. Ni and SO_4^{2-} promoters were co-impregnated to a parent zirconium hydroxide by a solution of $Ni(NO_3)_2 \cdot 6H_2O$ in H_2SO_4. After calcination at 948 K, the solids isomerized *n*-butane at 338 K. Up to 4.5 wt.% Ni content, nickel increases activity of $ZrO_2–SO_4^{2-}$, afterwards, the catalytic activity decreases. The temperature-programmed desorption of ammonia (TPD-NH_3) and IR of pyridine adsorbed results show that enhanced activity cannot be completely explained in function of a higher acid strength. The increase of the isomerizating activity is better explained in terms of a bimolecular mechanism, as proposed by Guisnet et al. [M.R. Guisnet, Acc. Chem. Res. 23 (1990) 392], involving olefins as intermediates. In this mechanism, Ni causes an enhancement in the surface concentration of olefins. In spite of the relatively high Ni concentration, X-ray diffraction results showed no evidence of any NiO phase due to this oxide is well-dispersed on the surface of $ZrO_2–SO_4^{2-}$ in form of small particles. The inhibition of isomerizating properties of the catalysts when hydrogen was present in the reactor feed confirmed this bimolecular mechanism. Interestingly, unpromoted $ZrO_2–SO_4^{2-}$ exhibited also the usual induction period observed on nickel-promoted sulfated zirconia catalysts. Then, this bimolecular mechanism for the *n*-butane isomerization could also apply in the unpromoted zirconia sulfate catalyst.

Keywords: Incipient wetness method; Nickel; *n*-Butane isomerization

1. Introduction

Catalytic cracking or isomerization of alkanes has been frequently used as a test reaction to asses the acidic properties of the solid acid catalysts. It has been shown that the slower the reaction, the stronger are the acid sites required for its catalysis. In this way, the minimum strength the acid sites must have for catalyzing each reaction has been estimated by comparing the change in the reaction rate as a function of the temperature of pyridine desorption [1]. Hence, the isomerization of 3,3-dimethyl-1-butene, which occurs very rapidly, requires weak acid sites just able to retain pyridine adsorbed above 493 K, whereas *n*-hexane transformation, which is 100 times slower, requires very strong

* Corresponding author. E-mail: harmenda@www.imp.mx

1381-1169/99/$ - see front matter
PII: S1381-1169(99)00172-7

acid sites capable of retaining pyridine adsorbed up to 793 K. These type of reactions could therefore be used to characterize the strength of the acid solids. However, the discovery that sulfated zirconia doped with iron and manganese catalyzes the isomerization of the *n*-butane even at room temperature [2,3], raises some fundamental questions on the nature of the active site or the mechanism of reaction responsible for these acid-catalyzed reactions.

Since the establishment that the acid-catalyzed isomerization of paraffins proceeds via a chain-carrying carbenium ion [4], the source of the initial carbocations is controversial. The easiness of the olefins in forming carbenium ions by simple protonation led to the hypothesis that trace amounts of olefins, introduced as impurities [5] or formed in situ by thermal cracking or dehydrogenation [6,7], could act as initiators. A second view is that carbocations could be generated by a direct attack of the paraffins by an acid site in three different ways: (i) a hydride abstraction by a Lewis site, (ii) a carbon–hydrogen bond attack, and, (iii) a carbon–carbon bond attack (protolysis). Although, in the case of paraffins as the sole reactant, the formation of carbonium ions with pentacoordinated carbon atoms has been showed by Haag and Dessau [8] to occur on strong acid sites, the term 'superacid' applied to ZrO_2–SO_4^{2-} have been recently questioned [9–11]. In this respect, it has been suggested that the remarkable catalytic activity of sulfate-doped zirconia is not caused by exceptionally strong acid sites, but by stabilization of a transition state complex at the surface [9]. A second mechanistic explanation [12–16] suggests that the presence of reducible oxides, incorporated at the sulfate-doped zirconia, leads to the intermediate formation of olefins. In this later case, the isomerization of *n*-butane would proceed via C_8^+ intermediates, which are known to easily undergo β-scission yielding fragments with *iso*-C_4 skeletons and also C_3 and C_5 alkanes.

In the present paper, we examined the catalytic behavior of the unpromoted and Ni-promoted ZrO_2–SO_4^{2-} solids in the *n*-butane isomerization reaction. All the sulfated zirconia catalysts used were capable to isomerize *n*-butane at 338 K. The acidity characterization of the samples by chemisorption of basic compounds showed no direct correlation between the acid strength and the catalytic properties of the solids. Our results confirm the idea of a bimolecular mechanism, in which Ni promotes the formation of olefins, which are intermediates of reaction, rather than the generation of stronger acid sites. Interestingly, when unpromoted ZrO_2–SO_4^{2-} was used, the isomerization of *n*-butane seems to be carried out through this same mechanism.

2. Experimental

2.1. Preparation of the solids

The unpromoted and Ni-promoted sulfated zirconia catalysts were prepared by the classical two-step method: first, precipitation of $Zr(OH)_4$ support, then sulfation. The parent zirconium hydroxide was precipitated from an aqueous solution containing 20 wt.% of $ZrCl_4$ (Aldrich, 99%) with an aqueous solution of ammonia (J.T. Baker, 28%) at room temperature, followed by washing with deionized water until the filtrate showed neutral pH. The resulting gels were dried at 393 K for 12 h. Then, the sulfate was incorporated by the incipient wetness impregnation technique with a solution of H_2SO_4 containing the appropriate amount of sulfate. In spite of a not so good homogeneity, the incipient wetness method let to have a better control of the quantity of promoters incorporated to the parent support. The impregnation time was 2 h and then the material was dried overnight at 393 K in a vacuum oven. The calcination was performed in air flow at 948 K for 1 h in a tubular furnace. In this way, the material designed as ZrS was obtained. Ni-promoted sulfated zirconia catalysts were obtained by impregnation of $Zr(OH)_4$ with an aqueous

solution of $Ni(NO_3)\cdot 2H_2O$ in H_2SO_4. Sulfur content was maintained at 4 wt.% of sulfate and the Ni content ranged from 0 to 9.6 wt.%. Both the time and of method of impregnation and the drying and calcination procedure were similar to those performed on unpromoted ZrO_2–SO_4^{2-}. The solids thus obtained were designed as *X* NiZrS where *X* represents the Ni content (wt.%) in the sample.

2.2. Characterization techniques

2.2.1. Chemical analysis

The sulfur content was measured by the combustion method. The gaseous products were analyzed using a LECO SC-44 instrument coupled to a microprocessor to obtain directly the sulfur content as wt.%. In all cases, the samples lost about 10% of sulfur initially charged. The 9.6NiZrS sample was not measured.

2.2.2. Surface area measurements

Surface area and pore size distributions were obtained from nitrogen isotherms determined at liquid nitrogen temperature on an automatic analyzer ASAP 2000 from Micromeritics.

2.2.3. Differential thermal analysis (DTA)

Differential thermal analysis was carried out in a Perkin-Elmer DTA 1700 instrument. DTA data were obtained from the dried sulfated zirconia samples at a heating rate of 10° min^{-1}. in a dried air flow (40 ml min^{-1}). Platinum crucibles were used as sample holders and Al_2O_3 was used as a reference material.

2.2.4. X-ray diffraction (XRD)

The powder XRD patterns were measured in a D-500 SIEMENS diffractometer with a graphite secondary beam monochromator and $CuK\alpha_2$ contribution was eliminated by the DIFFRAC/AC software to obtain a monochromatic $CuK\alpha_1$.

2.2.5. FT-IR studies

The solids were characterized by FT-IR spectroscopy using a 170-SX Nicolet spectrometer. Self supported wafers (14 mg) were mounted in a glass cell equipped with KBr windows, which permitted to follow the changes of the spectrum with thermal treatments. For the determination of acidity, the sample was evacuated to 10^{-1} Pa, then maintained under a flow (2.14 l h^{-1}) of nitrogen saturated with pyridine for 15 min. Outgassed 1 h at room temperature (pressure 10^{-1} Pa), then heated up to the desired temperature using linear program.

The concentration of Brønsted and Lewis acid sites was obtained by the Lambert–Beer law [17]. The absorbency (A_I) is determined as the integrated area under the curve as follows:

$$A_I = BC\int e_\nu\, d_\nu$$

where $\int e_\nu d_\nu$ is the extinction coefficient and it is proportional to 0.4343 (I_ν). In accord with Ref. [18], $I_\nu = 3.03$ cm μmol^{-1} or 3.26 cm μmol^{-1} for the bands at 1545 cm^{-1} and 1450 cm^{-1}, respectively. *B* is related to weight (g)/area (cm^{-2}) wafer ratio, and *C* is the concentration of the acid sites. So that, the concentration of Brønsted and Lewis acid sites can be calculated as:

$$C_{\text{Brønsted}} = \frac{A_I(1545\,\text{cm}^{-1})}{w(0.4343\times 3.03/\text{area})}$$

$$C_{\text{Lewis}} = \frac{A_I(1450\,\text{cm}^{-1})}{w(0.4343\times 3.26/\text{area})}.$$

2.2.6. Temperature-programmed desorption of ammonia (TPD-NH_3)

The total acidity of all the solids was measured by temperature-programmed desorption of ammonia. The solid was first saturated with a series of calibrated pulses of ammonia at 473 K, as described in the Altamira Instruments Notes [19]. Then, the NH_3 remained in the lines was carried under a dry nitrogen flow (30 ml min^{-1}) at the same temperature for 12 h. Subsequently, the temperature was raised up to 773 K (after this temperature, the thermal decomposition of

sulfates was carried out) with a heating rate of 10° min^{-1}. The NH_3 profile desorption was registered with a detector of thermal conductivity and the amount of ammonia retained by the solid at 473 K by the number of pulses required for the saturation of the surface of the solid.

2.2.7. Catalytic tests

The *n*-butane isomerization was performed at atmospheric pressure using an isothermal fixed-bed Pyrex reactor heated by a controlled temperature electric oven. Conditions of the catalytic test were: temperature = 338 K, WHSV = 0.4 h^{-1}, mass of catalyst = 1.0 g. The feed was either pure *n*-C_4 or *n*-C_4 diluted with hydrogen (5, 25 and 50 mole% of H_2). Prior to each reaction run, the catalyst was activated in situ by flowing dry air (40 ml min^{-1}) at 773 K for 1 h. Then it was cooled under air to the reaction temperature. The analysis of reaction products was done by on-line chromatography using a 3-m long, (1/8)″ diameter column packed with *n*-octane porasil.

3. Results and discussion

3.1. Chemical composition and textural parameters

Table 1 presents the physico-chemical characteristics of the solids. The nickel content was ranged from 0 to 9.6 wt.%, with the sulfate content remaining constant at 4 wt.%. After calcination at 948 K, the surface areas of these materials are in the range of 50–60 $m^2\ g^{-1}$. It is interesting to observe that up to 6 wt.% Ni content, the surface areas and the porosities of the samples remain practically constant. However, when Ni content increased until 9.6 wt.% (9.6NiZrS sample), the specific surface area and the total specific pore volume decrease dramatically with a concomitant increase in the mesoporosity (intraparticles) of the sample. These changes in the pore structure and surface area are all consistent with the market crystallite growth, and accompanying phase transformation, as a consequence of a sintering process that will be discussed later. It is noteworthy that at this greater nickel content, the sulfate does not maintain the surface area and porosity of the sample as generally reported [20–22]. This result suggests therefore, the presence of a weak interaction between the sulfate groups and the zirconia support in this sample. Probably at this great Ni concentration, there is a preferential adsorption of the nickel precursor on the support, which restrict the bonding of sulfate to zirconium hydroxide support.

3.2. DTA

Fig. 1 illustrates the DTA profiles of ZrO_2–SO_4^{2-} and Ni promoted ZrO_2–SO_4^{2-} samples. The endothermic peak observed about 413–433 K corresponds to removal of water adsorbed and the dehydroxilation of the hydrates. The wide exothermic peak centered at 843 K on unpromoted ZrO_2–SO_4^{2-} sample corresponds to

Table 1
Physico-chemical characteristics of the different samples

Sample	Chemical composition (wt.%)			Surface area ($m^2\ g^{-1}$)	Porous volume ($cm^3\ g^{-1}$)	Mean porous size (Å)
	ZrO_2	NiO	SO_4^{2-}			
ZrS	96.0	0	4	66	0.108	65
1NiZrS	95.0	1.0	4	62	0.108	70
1.5NiZrS	94.5	1.5	4	60	0.078	52
2.5NiZrS	93.5	2.5	4	56	0.083	39
4.5NiZrS	91.5	4.5	4	50	0.078	63
6NiZrS	90.0	6.0	4	66	0.072	44
9.6NiZrS	86.4	9.6	4	4	0.020	201

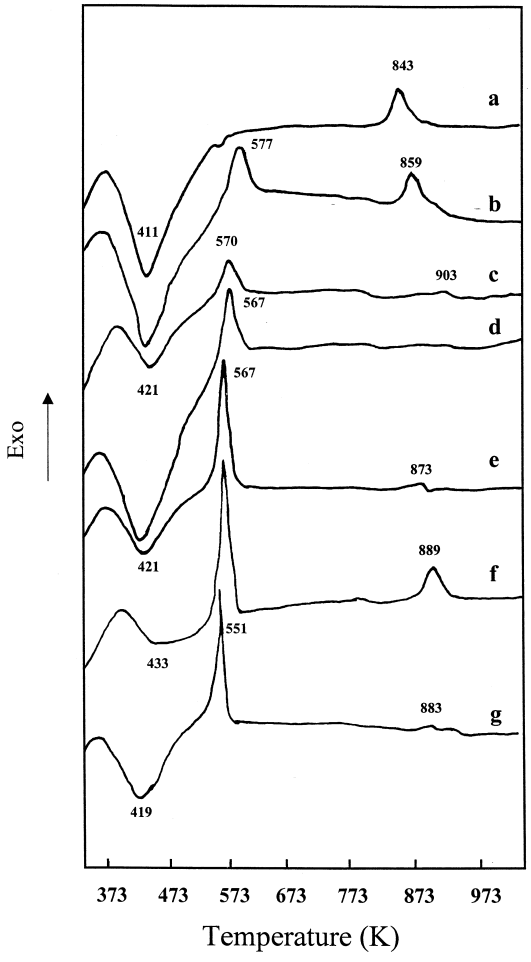

Fig. 1. DTA profiles for the unpromoted and Ni-promoted ZrO_2–SO_4^{2-} when heated in dried air: (a) ZrS, (b) 1NiZrS, (c) 1.5NiZrS, (d) 2.5NiZrS, (e) 4.5NiZrS, (f) 6NiZrS, (g) 9.6NiZrS.

a rearrangement of tetragonal ZrO_2 structure due to the activation of sulfur. We have shown [23,24] that this exothermic peak cannot be directly associated with the crystallization of ZrO_2. The incorporation of Ni to sulfated zirconia shifts this exothermic peak to higher temperatures and in some cases, it is not detectable. This suggests that there would be an associated effect of nickel and sulfate promoters in the stabilization of the tetragonal phase of ZrO_2, with all its inherent textural properties, at higher temperature. In Ni-promoted ZrO_2–SO_4^{2-} samples, a second exothermic peak at about 573 K was observed. Due to this, exothermic peak is not present in Ni-unpromoted sulfated zirconia, it is attributed to crystallization of NiO. The existence of such a glow exothermic peak is a well-documented feature of many metal oxides crystallization systems [25]. Richardson [26] has reported a temperature near to 573 K for the formation of NiO from $Ni(OH)_2$. From Fig. 1, we clearly see that this pick becomes more and more important and narrow as the Ni content is increasing.

3.3. Crystal structure

X-ray diffraction patterns taken after heating at 948 K are shown in Fig. 2. The X-ray pattern of the unpromoted sulfated zirconia reveals a well-crystallized tetragonal phase with a few percentage of monoclinic phase. In agreement with DTA results we can observe that the incorporation of nickel to sulfated zirconia stabilizes the tetragonal phase. The progressive decreasing of the peak that appears at the angle $2\theta = 28.2°$, assigned to the monoclinic phase, as the nickel content increases indicates that, in addition to sulfate, the presence of nickel stabilizes the metastable tetragonal phase of ZrO_2 at a higher temperature. It retards the sintering process of small crystals, which gives rise to the tetragonal to monoclinic phase transformation [27]. The

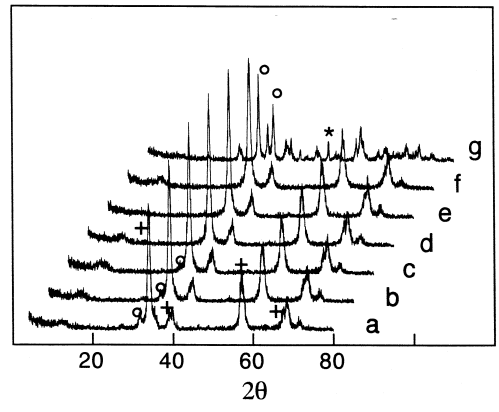

Fig. 2. X-ray diffraction patterns of unpromoted and Ni-promoted ZrO_2–SO_4^{2-} calcined at 948 K: (a) ZrS, (b) 1NiZrS, (c) 1.5NiZrS, (d) 2.5NiZrS, (e) 4.5NiZrS, (f) 6NiZrS, (g) 9.6NiZrS. (+) Tetragonal phase, (○) monoclinic phase, (*) NiO phase.

stabilization of the metastable tetragonal structure of ZrO_2 has been also reported to take place with the incorporation of many different metal oxides such as MgO, CaO, Se_2O_3, Y_2O_3, La_2O_3 and CeO [28]. Although it is generally accepted that the tetragonal phase is present in the highly acidic ZrO_2–SO_4^{2-} catalysts, it seems not play a direct role in the formation of the highly acidic sites present in this material as will be seen later. It is noteworthy that despite their significant concentration, we did not observe the lines of diffraction corresponding to any nickel oxide phase in the samples such as 4.5NiZrS and 6NiZrS, indicating the existence of a microcrystalline phase with a crystallite size smaller than 30 Å [29]. Only the sample with the higher Ni content (9.6NiZrS) shows one peak to $2\theta = 43.5°$, corresponding to the NiO phase. Interestingly, in this later sample, we also observed that the stabilization effect of sulfate and Ni promoters is not maintained, so the crystalline structure of ZrO_2 is majority monoclinic. These results indicate, in agreement with those of DTA profiles, that if at first NiO is formed, afterwards it probably remains on the surface of zirconia in form of small particles in spite of high temperature of calcination (948 K). Up to given concentration, the fact that a big particle of NiO was not observed suggests that there is a strong interaction between the sulfated zirconia and the NiO particles, which prevent the sintering of these later.

3.4. TPD-NH_3 and IR of pyridine adsorbed studies

3.4.1. Acidity from desorption ammonia

In spite of strong basicity of NH_3 molecule, which could measure acid sites with an insignificant contribution to catalytic activity, the thermal desorption of ammonia is a simple method widely used to investigate both the strength and the number of acid sites present on the surface of an acid solid. The results of this determination are summarized in Table 2. Clearly, it appears that the number of acid sites presents on ZrO_2–SO_4^{2-} samples is not affected by the presence of Ni. Indeed, we can see that the density of acid sites remains practically constant. In the 9.6NiZrS sample, the lost of acid sites is probably associated to the lost of sulfur (not measured), as evidenced by the sintering process observed by XDR. The ammonia thermal desorption profiles (not shown) present only one wide peak of desorption at about 573 K. This feature suggests, in a way, the presence of sites with different acid strength and, on the other hand, that these sites pose mainly as a medium acid strength [22]. Therefore, from these results emerge that our Ni-promoted or unpromoted ZrO_2–SO_4^{2-} cannot be considered as a superacid solid.

Table 2
Number of sites retaining ammonia at 373 K on the different samples

Sample	Ni content (wt.%)	Number of acid sites (meq-g^{-1})
ZrS	0	185
1NiZrS	1.0	162
1.5NiZrS	1.5	158
2.5NiZrS	2.5	171
4.5NiZrS	4.5	196
6NiZrS	6.0	257
9.6NiZrS	9.6	49

3.4.2. Acidity from IR of pyridine adsorption

Pyridine has been used as a probe for the determination of the acid sites nature present on the surface of the studied catalysts. The spectra observed after evacuation of pyridine at 323 K on the samples are reported in Fig. 3a. The stretching bands of infrared spectrum of pyridine adsorbed on solid acids have been clearly identify and reported [30]. The bands at 1455 and 1610 cm^{-1} correspond to different modes of vibration of pyridine coordinated to the Lewis acid sites. The band at 1545 cm^{-1} has been assigned to the pyridinium ion (Brønsted acid sites). Finally, the band at 1495 cm^{-1} is characteristic of the Lewis–Brønsted acid complex.

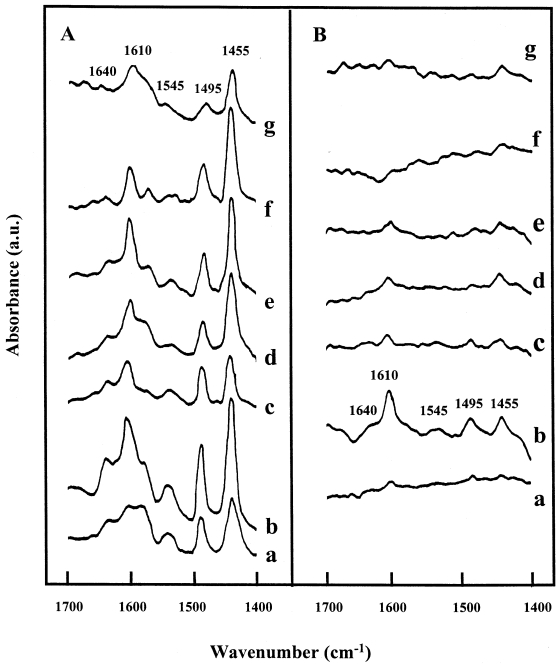

Fig. 3. Infrared spectra of pyridine adsorbed on the unpromoted and Ni-promoted ZrO_2–SO_4^{2-} calcined at 948 K: (a) ZrS, (b) 1NiZrS, (c) 1.5NiZrS, (d) 2.5NiZrS, (e) 4.5NiZrS, (f) 6NiZrS, (g) 9.6NiZrS. Pyridine adsorbed at room temperature, then evacuated at (A) 323 K and (B) 573 K.

On all the samples, we identify both types of acidity, with a greater contribution of Lewis acidity. Regardless of sample the intensities of all bands practically disappeared upon outgassing at 573 K (Fig. 3b), thus showing a moderate interaction between pyridine and the solids. Only for a Ni contents of 1 wt.% the general behavior remained with more intense bands, the positions of which were unchanged. Trying to find a possible correlation between the Ni content and the acid strength of the samples, the peak areas corresponding to Brønsted and Lewis sites after evacuation at 323 and 573 K were determinated. These areas as well as the Brønsted to Lewis ratio (B/L) for each catalyst are summarized in Table 3. Taken into account that the extinction coefficient of protonated and coordinated pyridine could not be the same, from the (B/L) ratio we observe a more important increasing in the density of Lewis sites than Brønsted sites when Ni-promoter appears. The comparison of B/L ratio after outgassing at 323 and 573 K evidences a higher lost of Lewis sites than Brønsted sites.

Table 3
Brønsted and Lewis acid sites measured by IR of adsorbed pyridine

Sample	mmol Py g^{-1} ($T = 323$ K)			mmol Py g^{-1} ($T = 573$ K)		
	Brønsted	Lewis	Ratio B/L	Brønsted	Lewis	Ratio B/L
ZrS	35	97	0.360	4	9	0.444
1NiZrS	49	176	0.278	18	23	0.782
1.5NiZrS	45	181	0.248	10	14	0.714
2.5NiZrS	36	189	0.190	4	36	0.111
4.5NiZrS	34	207	0.164	7	16	0.437
6NiZrS	16	170	0.094	0	13	0
9.6NiZrS	9	98	0.091	0	24	0

3.5. Catalytic n-butane isomerization

The catalytic data of the conversion of *n*-butane as a function of time on stream are shown in Fig. 4 for SZr and the NiZrS solids series. Isobutane was the main product (> 90% selectivity) while propane and isopentane were the secondary ones. All the catalysts showed an induction period, the activity passes through a maximum with time on stream followed by deactivation. Similar induction period has also been reported by others authors on sulfated

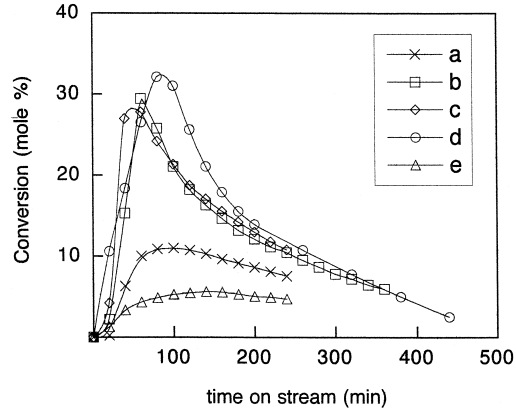

Fig. 4. *n*-Butane isomerization conversion as a function of time on stream over unpromoted and Ni-promoted ZrO_2–SO_4^{2-} calcined at 948 K: (a) ZrS, (b) 1NiZrS, (c) 1.5NiZrS, (d) 4.5NiZrS, (e) 6NiZrS. Temperature of reaction = 338 K, WHSV = 0.4 h^{-1}.

zirconia promoted with different metals [13–15]. According to the hypothesis of bimolecular mechanism, this initial induction period would be ascribed to a build-up of olefins on the catalyst surface. It was interesting that our unpromoted sulfated zirconia (with maximum of conversion near to 5 mole%, even at this low temperature, 338 K) showed this induction period. This fact suggests that the *n*-butane isomerization on unpromoted ZrO_2–SO_4^{2-} is carried out through the same bimolecular mechanism, therefore, it implies a dehydrogenation process on this unpromoted solid. Different trends were observed as nickel was added to sulfated zirconia. From Fig. 4, it can be observed that the incorporation of 1 wt.% of nickel strongly enhances the activity of ZrO_2–SO_4^{2-}. On increasing the Ni content to 1.5 and 4.5 wt.%, we did not observe a great difference in the catalytic behavior among these three samples. A further increase in Ni content up 6 wt.% decreases again the catalytic activity. Finally, the sample with the greater amount of nickel (9.6NiZrS) was completely inactive under our reaction conditions, due to the lost of sulfur associated to the tetragonal to monoclinic phase transformation. It can also be observed that the higher the activity showed by the catalyst, more severe is its deactivation. If some differences in the density of acid sites were observed among the seven catalysts investigated, a direct correlation with catalytic activity was not apparent. For example, the unpromoted sulfated zirconia (ZrS), which is significatively less active than 1 wt.% Ni promoted sulfated zirconia (1NiZrS), showed a greater density of acid sites measured by TPD-NH_3 (Table 2).

On the other hand, when we correlate both the nature and the density of acid sites, measured by IR of pyridine adsorbed, with the catalytic activity a different behavior was found. From the curves of Fig. 5, it seems to be a correlation between the density of Lewis acid sites and the activity of the samples. As the Ni content increase, we observed a maximum in the density of Lewis acid sites for a 4.5 wt.% Ni

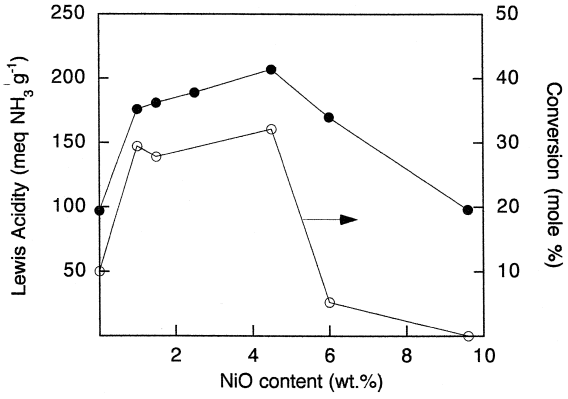

Fig. 5. *n*-Butane isomerization conversion and Lewis acidity as a function of NiO content in Ni-promoted ZrO_2–SO_4^{2-}. (○) Conversion, (●) Lewis acidity.

content. This maximum corresponds to that of the catalytic activity showed by the solids. But in this point, as in the case of TPD-NH_3, we observed that 6NiZrS sample, with practically the same density of Lewis acid sites than 1NiZrS sample, is about 6 times less active catalyst.

In the literature, there are several attempts to correlate the acidity (Brønsted or Lewis) with the catalytic performance of sulfated zirconia. On unpromoted ZrO_2–SO_4^{2-}, Nascimento et al. [31] have proposed that its isomerizing activity can be related to the simultaneous presence of Brønsted and Lewis acid sites. In fact, they observe that the maximum *n*-butane isomerization activity is obtained when the (B/L) ratio is about 1. Hsu et al. [2] showed that sulfated zirconia activity could be significantly enhanced by the addition of Fe and Mn. They establish that this enhancement was due to the generation of additional sites, with higher acid strength than those on unpromoted sulfated zirconia. In our case, nevertheless, the density of Lewis acid sites passes through a maximum with nickel content (as that showed by catalytic activity), it appears that the modification of the acid sites density is not the main factor that explains the increase in activity of Ni-promoted sulfated zirconia catalysts. These results would favor the idea that the isomerization of *n*-butane on ZrO_2–SO_4^{2-}, promoted or not, is carried out

Table 4
n-Butane conversion over 4.5NiZrS catalyst at 338 K, and atmospheric pressure

H_2 / *n*-C_4 molar ratio in feed	Conversion (mole%)
0	26.53
0.05	2.80
0.50	0

WHSV = 0.37 h^{-1}.

through a bimolecular mechanism. As mentioned by several authors [14,32–35], the role of metallic promoter will be to act as dehydrogenation sites. The olefins thus generated would participate in the subsequent dimerization step. However, our results show that among 1 to 4.5 wt.% Ni content, the activity seems to be independent of Ni content, which suggests that the dehydrogenation of butane is not the rate limiting step for the *n*-butane isomerization. So, we support the idea of Coelho et al. [13] and Tabora and Davis [34], in which they suggest that the transition metal may attract olefin molecules to form a butene pool that enhances the surface concentration of olefins near to the acid sites. Under these conditions, the dimerization step, as the rate step limiting, would be accelerated by the higher surface concentration of olefins.

The idea of the olefins as intermediates of reaction is consistent with the fact that the slow induction period observed on unpromoted ZrO_2–SO_4^{2-} (Fig. 4) is greatly enhanced by the incorporation of Ni. One increase of reaction temperature also causes the same effect. It is explained as an effect kinetic as reported by Resasco et al. [15,35]. According to this hypothesis the rate of *n*-butane isomerization would be inhibited when it was carried out under an hydrogen atmosphere. Indeed, in Table 4 we can see as the maximum of activity decreased as the partial pressure of H_2 was increased. It is consistent with a lower reaction rate. However, as reported by Garin et al. [36], it is possible that the mechanism of reaction that proceeds under hydrogen could be different than that with sole *n*-butane as feed.

Given that the acidity of sulfated zirconia, measured by the adsorption of NH_3 or pyridine, could be considered as a medium acid strength, the dehydrogenating capacity of ZrO_2–SO_4^{2-} could be better explained by the acid–base properties of ZrO_2, which have been shown by Feng et al. [37] and recently by Coman et al. [38]. These will greatly enhanced by the addition of sulfate and nickel promoters to zirconium hydroxide support.

4. Conclusions

As conclusions, we can establish the following.

(1) A relatively easy coimpregnation of Ni and SO_4^{2-} promoters to a zirconium hydroxide support was used to obtain a sulfated zirconia catalyst, which is capable to isomerize the *n*-butane at 338 K.

(2) Although our *n*-butane isomerization on Ni/ZrO_2–SO_4^{2-} study showed the importance of the olefins formation as reaction intermediates, the dehydrogenating properties of NiO is not the main factor responsible for the different catalytic behavior between the unpromoted and Ni-promoted sulfated zirconia. The increase of Lewis acid sites density of ZrO_2–SO_4^{2-} as Ni is present suggests that Ni could increase the strength of the acid–base pair of sulfate zirconia, hence increasing its dehydrogenating properties.

References

[1] G. Bourdillon, C. Gueguen, M. Guisnet, Appl. Catal. 61 (1990) 123.
[2] C.Y. Hsu, C.R. Heimbruch, C.T. Armes, B.C. Gates, J. Chem. Soc. Chem. Commun. (1992) 1645.
[3] J.E. Tabora, R.J. Davis, J. Chem. Soc. Faraday Trans. 91 (12) (1995) 1825–1833.
[4] H.S. Bloch, H. Pines, L. Schmerling, J. Am. Chem. Soc. 67 (1975) .
[5] D.A. McCaulay, J. Am. Chem. Soc. 81 (1959) 6437.
[6] A. Brenner, P.H. Emmet, J. Catal. 75 (1982) 221.

[7] D.M. Anufriev, P.N. Kuznetsov, K.G. Ione, J. Catal. 65 (1980) 221.
[8] W.O. Haag, R.M. Dessau, Proceedings 8th International Congress on Catalysis, Berlin, 1984, Vol. II, Dechema, Frankfurt-am-Main, 1984, p. 305.
[9] B. Umansky, J. Engelhart, W.K. Wall, J. Catal. 127 (1991) 128.
[10] L.M. Kustov, V.B. Kazansky, F. Figueras, D. Tichit, J. Catal. 150 (1994) 143.
[11] V. Adeeva, J.W. de Haan, J. Jänchen, G.D. Lei, V. Schünemann, L.J.M. van de Ven, V.M.H. Sachtler, R.A. van Santen, J. Catal. 151 (1995) 364.
[12] J.C. Yori, J.M. Parera, Appl. Catal. A 147 (1996) 145.
[13] M.A. Coelho, D.E. Resasco, E.C. Sikabwe, R.L. White, Catal. Lett. 32 (1995) 253.
[14] V. Adeeva, G.D. Lei, W.M.H. Sachtler, Appl. Catal. 118 (1994) L11.
[15] D.E. Resasco, H. Liu, W.E. Alvarez, Actas XV Simposio Iberoamericano de Catálisis, Vol. 1, Cordoba, Argentina, 1996, p. 191.
[16] C.R. Vera, J.C. Yori, J.M. Parera, Appl. Catal. 167 (1) (1998) 75.
[17] E.A. Paukshtis, E.N. Yurchenko, Russ. Chem. Rev. 52 (1983) 3.
[18] T.R. Hughes, H.M. White, J. Phys. Chem. 71 (1967) 7.
[19] Altamira Instruments Notes, November, 1994.
[20] R. Srinivasan, D. Taulbee, B.H. Davis, Catal. Lett. 9 (1991) 1.
[21] R. Srinivasan, C. Hubbard, O.B. Covin, B.H. Davis, Chem. Mater. 5 (1993) 27.
[22] A. Corma, V. Fornes, M.I. Juan-Rajadell, J.M. Lopez-Nieto, Appl. Catal. A 16 (1994) 151.
[23] H. Armendáriz, B. Coq, D. Tichit, R. Dutartre, F. Figueras, J. Catal. 173 (1998) 345.
[24] H. Armendáriz, C. Sanchez-Sierra, F. Figueras, B. Coq, C. Mirodatos, F. Lefevre, D. Tichit, J. Catal. 171 (1997) 85.
[25] P.D.L. Mercera, J.G. van Ommen, E.B.M. Doesburg, A.J. Burggraaf, J.R.H. Ross, Appl. Catal. A 71 (1991) 363.
[26] J.T. Richardson (Ed.), Principles of Catalyst Development, Plenum, New York, 1989, p. 140.
[27] R.C. Garvie, J. Phys. Chem. 82 (1985) 218.
[28] P.D.L. Mercera, J.G. van Ommen, E.B.M. Doesburg, A.J. Burggraaf, J.R.H. Ross, Appl. Catal. A 57 (1990) 127.
[29] H.P. Klug, L.E. Alexander (Eds.), X-ray Diffraction Procedures, Wiley, New York, 1967.
[30] J. Ward, in: J.A. Rabo (Ed.), Zeolite Chemistry and Catalysis, ACS, Monograph 171, Am. Chem. Soc., Washington, DC, 1976.
[31] P. Nascimento, C. Akratopoulou, G. Coudurier, C. Travers, J.F. Joly, J.C. Vedrine, in: F. Guczi, F. Solymosi, P. Tétényi (Eds.), Proceedings 10th International Congress on Catalysis, Budapest, 1992, Akadémiai Kiado, Budapest, 1993, p. 1185.
[32] M. Hino, K. Arata, Catal. Lett. 30 (1995) 25.
[33] E. Iglesia, S.L. Soled, G.M. Kramer, J. Catal. 144 (1993) 238.
[34] J.E. Tabora, R.J. Davis, J. Catal. 162 (1996) 125.
[35] D.E. Resasco, H. Liu, W.E. Alvarez, Appl. Catal. A 162 (1997) 103.
[36] F. Garin, D. Andriamasinoro, A. Abdulsamad, J. Sommer, J. Catal. 131 (1991) 199.
[37] Z. Feng, W.S. Postula, A. Akgerman, R.G. Anthony, Ind. Eng. Chem. Res. 34 (1995) 78.
[38] S. Coman, V. Pârvulescu, P. Grange, V.I. Pârvulescu, Appl. Catal. A 176 (1999) 45.